ARTICLE   OPEN

Check for updates

Pyrite-based denitrification combined with electrochemical disinfection to remove nitrate and microbial contamination from groundwater

Eleftheria Ntagia [1 ✉] and Piet Lens[1]

Nitrate and microbial contamination of groundwater can occur in countries that face intense urbanization and inadequate sanitation. When groundwater is the main drinking water source, as is often the case in such countries, the need to remove these contaminants becomes acute. The combination of two technologies is proposed here, a biological step to denitrify and an electrochemical step to disinfect the groundwater, thereby aiming to reduce the chemical input and the footprint of groundwater treatment. As such, a pyrite-based fluidized bed reactor (P-FBR) was constructed to autotrophically denitrify polluted groundwater. The P-FBR effluent was disinfected in an electrochemical cell with electrogenerated Cl_2. Nitrate was removed with 79% efficiency from an initial 178 mg NO_3^- L^{-1} at an average denitrification rate of 171 mg NO_3^- L^{-1} d^{-1}, with 18 h hydraulic retention time (HRT). The electrochemical unit achieved a 3.8-log reduction in total coliforms with a 41.7 A h m^{-3} charge density.

INTRODUCTION

Groundwater constitutes the main potable water source in low-income countries, greatly in Sub-Saharan countries, where the share for agricultural and industrial sectors is low, as well as in countries such as Ireland and the UK where these sectors are primarily rainfed[1,2]. The main pressors for groundwater quality deterioration are poor sanitation facilities, uncontrolled release of ailing treated domestic and industrial wastewater, cattle farming with uncontrolled manure spreading and intense fertilizing activities. Local conditions can intensify groundwater pollution, such as vulnerable aquifers and the intensification of extreme weather conditions[1,3–5].

Elevated concentrations of nitrate (NO_3^-), chloride (Cl^-), as well as microbial indicators such as fecal and total coliforms (TC) suggest anthropogenic groundwater pollution. Nitrate concentrations as high as 500 mg NO_3^- L^{-1} have been reported in peri-urban areas of low-income countries, alongside with 300 mg Cl^- L^{-1} and 2 log CFU 100 mL^{-1} *Escherichia coli* (*E. coli*) and 4 log CFU 100 mL^{-1} TC[4–6]. The concentrations vary largely with the local geological conditions and with the source of contamination. As a way to tackle waterborne diseases, the WHO has set a maximum of 50 mg NO_3^- L^{-1} and 0 CFU 100 ml^{-1} for TC in drinking water[7].

Groundwater is poor in organic content, therefore conventional treatment schemes including heterotrophic denitrification are not financially sustainable. An option is to target autotrophic groundwater denitrification with electron donors such as hydrogen gas (H_2), elemental sulfur (S^0), sulfide (HS^-), thiosulfate ($S_2O_3^{2-}$), ferrous iron (Fe^{2+}) or even pyrite (FeS_2)[8,9]. Based on the respective stoichiometric equations the denitrification capacities range from 2.5 g NO_3^--N g^{-1} e$^-$ donor for H_2 to 0.05 and 0.1 g NO_3^--N g^{-1} e$^-$ donor for reduced iron (Fe^{2+} and Fe^0)[9,10]. Pyrite driven denitrification occurs naturally in aquifers[11–14] and FeS_2 oxidation is coupled to microbial NO_3^- reduction to nitrogen gas (N_2), with a 3 mol NO_3:1 mol FeS_2 stoichiometric ratio, accompanied by the production of 2 mol SO_4^{2-}[12,15]. Furthermore, FeS_2 has been utilized in low C/N wastewater treatment[16,17], as well as in

groundwater denitrification, mainly in bottle tests[18,19]. Pyrite is a ubiquitous, low-cost mineral that is frequently found as a waste product of mining activities[20]. Additionally, during FeS_2 denitrification a circum-neutral pH is maintained, resulting in minimization of chemical inputs for this process[17,18].

In addition to denitrification, polishing steps are required to provide safe drinking or irrigation water, as the microbial load of the denitrified effluent, will not allow for direct consumption or reuse[21]. Several disinfection practices have been used so far to polish water treatment effluents and chemical oxidation, either with free chlorine, ozone (O_3) or UV, is generally preferred for potable water reuse[22]. However, alternative disinfection methods are being sought to provide the treatment process with chemical and grid independency, including electrochemical disinfection, also referred to as electrochlorination when free chlorine is the chemical agent produced[23]. In electrochlorination, chloride ions (Cl^-) naturally contained in groundwater are oxidized to chlorine (Cl_2) at the surface of an electrode, when a constant source of current is applied by an external power source[24,25]. The produced Cl_2 mixes with the bulk electrolyte and undergoes hydrolysis, producing two potent disinfectants: hypochlorous acid (HOCl) and hypochlorite (OCl$^-$). The ratio of the two is determined by the solution pH[26,27]. Electrochemical disinfection has been tested for directly treating groundwater or irrigation water contaminated with pathogens[28–30], but also as a polishing step for bioreactor effluents[27,31]. The disinfection efficiency will depend upon the anode material, the Cl^- concentration of the electrolyte, the pH and upon the organics and ammonia content of the water to be treated[22].

This study combined continuous autotrophic denitrification with FeS_2 as electron donor and electrochemical disinfection through Cl^- oxidation to Cl_2 (HOCl + OCl$^-$) to treat groundwater. Here, polluted groundwater was treated in a pyrite-based fluidized bed reactor (P-FBR) and the P-FBR effluent was disinfected through chlorination in the anodic compartment of the electrochemical cell. The efficiency of FeS_2-based autotrophic

---

[1]National University of Ireland, Galway, University Road, H91 TK33 Galway, Ireland. ✉email: ele.ntagia@gmail.com

denitrification at ambient conditions and at high Cl^- concentrations was investigated aiming for long-term FeS_2 denitrification of real groundwater. Furthermore, the electrochlorination efficiency with Pt/Ti electrodes and the effect of the real groundwater matrix on electrochlorination were studied. The electrochemical disinfection efficiency of the FeS_2 denitrified effluents was finally tested.

RESULTS

Continuous denitrification of synthetic groundwater in the pyrite-based fluidized bed reactor (P-FBR)

The biological step was a denitrification FBR with a pyrite (FeS_2) bed as electron donor (P-FBR). The P-FBR was inoculated and operated in batch with synthetic polluted groundwater (SGW) until NO_3^- was eliminated (details provided in the Methods section). The first batch lasted seven days (Fig. 1) and 44 mg NO_3^- L^{-1} d^{-1} was the highest nitrate removal rate achieved. Within the first three days, the NO_3^- decrease was accompanied by a NO_2^- increase, which was then consumed, indicating complete denitrification of NO_3^- to N_2 gas. Between days 7 and 23, several batch cycles took place to determine the denitrification rates and determine the hydraulic retention time (HRT) for the continuous operation (data not shown).

Starting on day 23, the P-FBR was operated in continuous mode for 41 days with SGW (Fig. 1). During this operation three different HRTs were tested, 24, 12 and 18 h, aiming to both achieve an effluent NO_3^- concentration lower than 50 mg NO_3^- L^{-1} and also to minimize the groundwater treatment time. The denitrification rate achieved at 24 h HRT was 167.9 (±7.5) mg NO_3^- L^{-1} d^{-1} (94.3 ± 4.2% NO_3^- removal efficiency) and the effluent NO_3^- concentration was 10.1 (±7.5) mg NO_3^- L^{-1} (Table 1). When the HRT

was decreased to 12 h, the NO_3^- removal rate decreased to 93.2 (±37.0) mg NO_3^- L^{-1} d^{-1} (76.2 ± 10.4% NO_3^- removal efficiency) and the NO_3^- effluent concentration increased to 42.4 (±18.5) mg NO_3^- L^{-1}. During that period, NO_2^- started accumulating, up to 6.4 (±8.4) mg NO_2^- L^{-1}, signifying incomplete denitrification due to the increased NO_3^- loading rate at the decreased HRT. At HRT 18 h, denitrification rates resumed to an average 134.7 (±14.1) mg NO_3^- L^{-1} d^{-1} (81.8 ± 6.0% NO_3^- removal efficiency), with 32.5 (±10.6) mg NO_3^- L^{-1} effluent concentrations, always below the maximum allowed drinking water levels[7]. Higher NO_2^- concentrations were measured during that period, on average 22.0 (±15.1) mg NO_2^- L^{-1}. However, this could be attributed to the 12 h HRT operation effect, which is also confirmed by the absence of NO_2^- in the subsequent operational periods with real groundwater. The pH remained stable at 7 at all three HRT tested with SGW (7.3 ± 0.1, 7.1 ± 0.1 and 7.0 ± 0.0 at respectively 24, 12 and 18 h HRT), without chemical dosing for pH control.

Continuous denitrification of real groundwater in the pyrite-based fluidized bed reactor (P-FBR)

After establishing a stable, continuous P-FBR operation with SGW at 18 h HRT, the influent was switched to real groundwater (GW) and the P-FBR was operated for 35 days, completing three treatment cycles with GW with different Cl^- and TC loads (Table 2, Methods section). During these 35 days of operation with GW a stable denitrification performance was maintained with an average denitrification rate of 171 mg NO_3^- L^{-1} d^{-1} (average NO_3^- loading rate was 215 mg NO_3^- L^{-1} d^{-1}) for all three cycles, corresponding to an average 79% denitrification efficiency for the three cycles with GW (Table 1). Accordingly, the average effluent NO_3^- concentration was 33 mg NO_3^- L^{-1}, meeting the standard
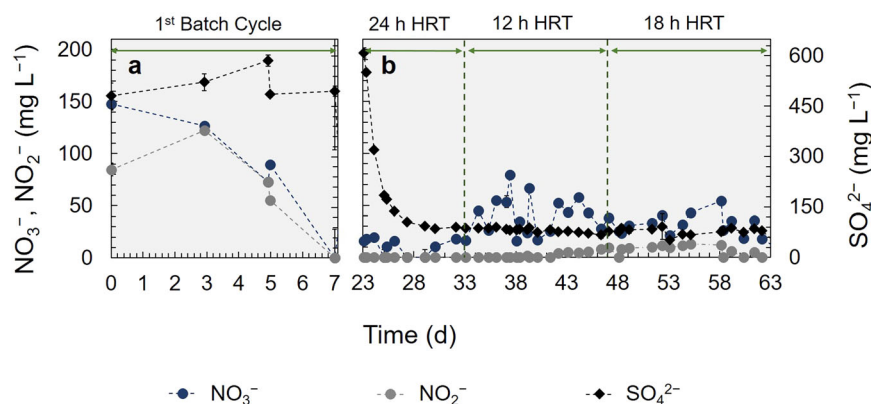

Fig. 1 Total operational period of the P-FBR denitrification reactor with synthetic polluted groundwater (SGW). a First batch operational cycle (days 0–7) and **b** continuous operation (days 23–64) with 24 h, 12 h and 18 h HRT. The error bars represent the standard deviation of $n = 3$ analytical replicates.

Table 1. Denitrification efficiency of the pyrite-based fluidized bed reactor (P-FBR) during continuous operation with synthetic (SGW) and real (GW) groundwater.

| Operational cycle	HRT [h]	Effluent concentrations [mg L^{-1}]				NO_3^- removal efficiency [%]	NO_3^- removal rate [mg NO_3^- L^{-1} d^{-1}]	Effluent electrical conductivity [mS cm^{-1}]
		NO_3^-	NO_2^-	Cl^-	SO_4^{2-}			
SGW-Cycle I	24	10.1 ± 7.5	0.0 ± 0.0	345.9 ± 36.5	99.8 ± 17.6	94.3 ± 4.2	167.9 ± 7.5	2.1 ± 0.3
SGW-Cycle II	12	42.4 ± 18.5	6.4 ± 8.4	293.4 ± 40.2	80.0 ± 6.1	76.2 ± 10.4	93.2 ± 37.0	2.0 ± 0.1
SGW-Cycle III	18	32.5 ± 10.6	22.0 ± 15.1	274.3 ± 29.0	77.0 ± 10.6	81.8 ± 6.0	134.7 ± 14.1	1.9 ± 0.1
GW-Cycle I	18	24.1 ± 8.3	0.8 ± 2.3	93.0 ± 9.4	27.8 ± 4.8	85.5 ± 5.3	175.6 ± 27.7	0.9 ± 0.0
GW-Cycle II	18	40.6 ± 8.1	0.0 ± 0.0	268.2 ± 41.0	26.9 ± 1.5	76.6 ± 8.1	163.8 ± 22.4	1.8 ± 0.2
GW-Cycle III	18	33.7 ± 18.6	0.0 ± 0.0	275.7 ± 75.5	28.1 ± 2.6	75.7 ± 10.3	173.4 ± 30.3	2.7 ± 0.9
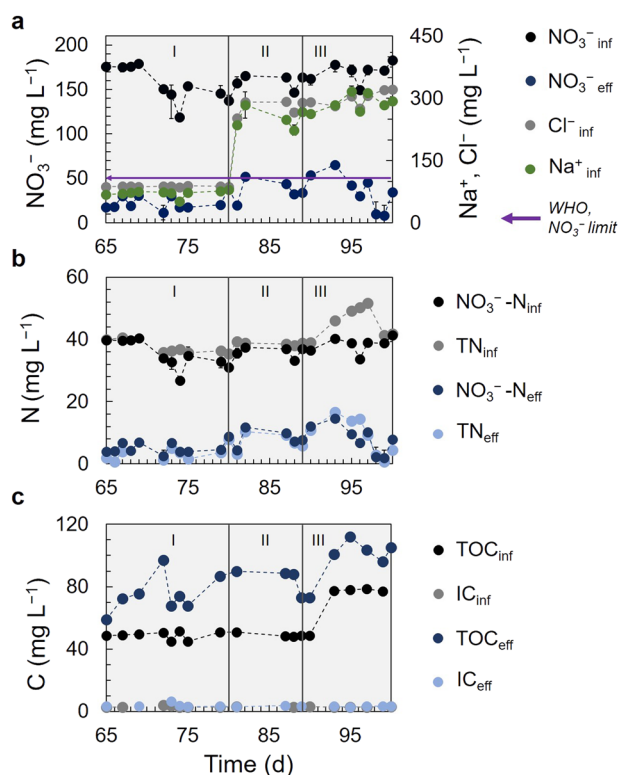
Fig. 2 P-FBR operational performance with real groundwater (GW) (days 65–100). a NO_3^- removal and changes after Cl^- and Na^+ increase observed in GW-Cycles II and III, **b** total nitrogen (TN) and nitrate nitrogen (NO_3^--N) and **c** total organic carbon (TOC) and inorganic carbon (IC), in the influent and effluent of the P-FBR. The error bars represent the standard deviation of $n = 3$ analytical replicates.

for reuse as potable water and furthermore, NO_2^- was not detected at any of the GW operational cycles.

Although the denitrification rates along the three cycles with GW did not present significant changes, a marginal decrease in the denitrification rate, alongside with a marginal increase in the effluent NO_3^- concentration were observed after day 80 (Fig. 2a and Table 1). On day 80, the GW-Cycle II started, where the Cl^- concentration was increased from 93 to 268 mg Cl^- L^{-1}, similar to the initial operation with SGW (Fig. 2a and Table 1), accompanied with an increase in the Na^+ concentration from an average 77 to 234 mg Na^+ L^{-1}. This greater concentration of NaCl negatively affected the denitrifying activity in the P-FBR, however, denitrification was not inhibited and after 15 days of operation at higher Cl^- concentrations (day 95 in Fig. 2a), the performance recovered with a NO_3^- effluent concentration below the limit of 50 mg NO_3^- L^{-1}.

The GW only contained a low amount of ammonium nitrogen, as almost all of the total nitrogen (TN) was measured as NO_3^--N in both the influent and the effluent of the P-FBR (Fig. 2b). However, the GW presented a higher organic load, 48.7 (±2.8) mg TOC L^{-1} for GW-Cycle I, 48.3 (±0.3) mg TOC L^{-1} for GW-Cycle II and 77.7 (±0.3) mg TOC L^{-1} for GW-Cycle III (Fig. 2c), compared to SGW that had no organic content. In GW-cycle III, this higher TOC load can also partially be attributed to the higher TC load, 500 MPN 100 mL^{-1}, compared to 7 and 2 MPN 100 mL^{-1} in GW-Cycles I and II, naturally contained in the GW and no microbial load in the SGW. The TOC concentration was consistently higher in the effluent than in the influent, 77.2 (±10) mg TOC L^{-1} in GW-Cycle I, 83.2 (±7.3) mg TOC L^{-1} in GW-Cycle II and 103.5 (±5.2) mg TOC L^{-1} in GW-Cycle III, indicating a release of organic matter in the denitrified groundwater.

The SO_4^{2-} concentration was marginally higher in the effluent than in the influent, except for GW-Cycle III. The influent SO_4^{2-} concentration was 25.9 (±3.4) mg L^{-1}, 25.7 (±0.6) mg L^{-1} and 30.4 (±0.6) mg L^{-1} and the effluent SO_4^{2-} concentration was 27.8 (±4.8) mg L^{-1}, 26.9 (±1.5) mg L^{-1} and 28.1 (±2.6) mg L^{-1}, in GW-Cycles I, II and III, respectively (Supplementary Table 1). The concentration of all cations remained unchanged between the influent and the effluent of the P-FBR (Supplementary Table 2), apart from potassium (K^+). The influent K^+ concentration in GW-Cycle I and II was close to and below the ICP detection limit, respectively, whilst in GW-Cycle III it was 3.6 (±0.5) mg L^{-1}. However, in the effluent, 2.1 (±0.9), 1.2 (±0.6) and 5.4 (±1.0) mg K^+ L^{-1} were detected in GW-Cycles I, II and III, respectively, (Supplementary Table 2 and Supplementary Fig. 1), consistently higher than the K^+ in the P-FBR influent. The pH remained stable at 7.3 during GW treatment without any chemical addition for pH control. The Cl^- concentration, essential for the subsequent disinfection step, remained also unchanged between influent and effluent of the P-FBR (Table 1). Small changes in the organic content, the concentration of anions and cations or the pathogens load between the influent and effluent of the P-FBR did not affect the conductivity and resulted in an effluent conductivity of 1.8 (±0.2) and 2.7 (±0.9) mS cm^{-1}, for GW-Cycles II and II, respectively (Table 1 and Supplementary Table 1).

Electrochlorination efficiency evaluated with denitrified groundwater

Batch, three-hour electrolysis experiments were conducted at 50 mA constant current ($j = 2$ mA cm^{-2}) to investigate Cl_2 evolution at the Pt/Ti anode with the SGW P-FBR effluent (Fig. 3a, b) and the GW-Cycle III P-FBR effluent (Fig. 3c, d). The initial Cl^- concentration for the two tests was similar, i.e. 289 (±6.5) mg Cl^- L^{-1} and 295.2 (±0.9) mg Cl^- L^{-1} for SGW and GW, respectively, while the two effluents differed in initial TOC concentration. This resulted in differences in measurable free and total chlorine as well as in the calculated respective chlorine production rates (Fig. 3a, c). Chlorine was produced with SGW at 1.65 (±0.05) V vs Ag/AgCl anode potential and with GW-Cycle III effluent at 1.43 (±0.01) V vs Ag/AgCl anode potential.

During constant current electrolysis with SGW the free and total chlorine increased with run time resulting in 0.455 (±0.002) mg L^{-1} final free chlorine concentration and 0.640 (±0.005) mg L^{-1} total chlorine. The production rate obtained was 3.89 mg L^{-1} d^{-1} free chlorine and 5.66 mg L^{-1} d^{-1} total chlorine (Fig. 3a). The production rates remained stable between the first and second hour of operation, at 4.12 and 4.09 mg L^{-1} d^{-1} for free chlorine and 6.37 and 7.24 mg L^{-1} d^{-1} for total chlorine for the first and second hour, respectively, while they dropped in the last hour to 3.46 mg L^{-1} d^{-1} free and 3.38 mg L^{-1} d^{-1} total chlorine. The pH dropped from initially pH 7.90 to 6.74 at which 85% of the free chlorine is present as HOCl and the remaining as OCl$^-$[26]. Similarly, the alkalinity and conductivity decreased from an initial 239.4 (±3.7) mg L^{-1} as $CaCO_3$ to a final 53.9 (±1.2) mg L^{-1} as $CaCO_3$ and from initially 2.1 (±0.0) mS cm^{-1} to a final conductivity of 1.8 (±0.0) mS cm^{-1} (Fig. 3b).

After the three-hour GW-Cycle III effluent test, the measured free chlorine concentration was 0.132 (±0.001) mg L^{-1} and the total chlorine was 0.423 (±0.003) mg L^{-1}. The production rate for free chlorine was of 0.56 mg L^{-1} d^{-1} and for total chlorine, it was 2.12 mg L^{-1} d^{-1} (Fig. 3c). The pH dropped from initially 7.96 to 6.83. Accordingly, the alkalinity and conductivity decreased from an initial 418.3 (±4.3) mg L^{-1} as $CaCO_3$ to a final 187.9 (±4.1) mg L^{-1} as $CaCO_3$ and from an initial 2.1 (±0.0) mS cm^{-1} to a final 1.7 (±0.0) mS cm^{-1} conductivity (Fig. 3d).
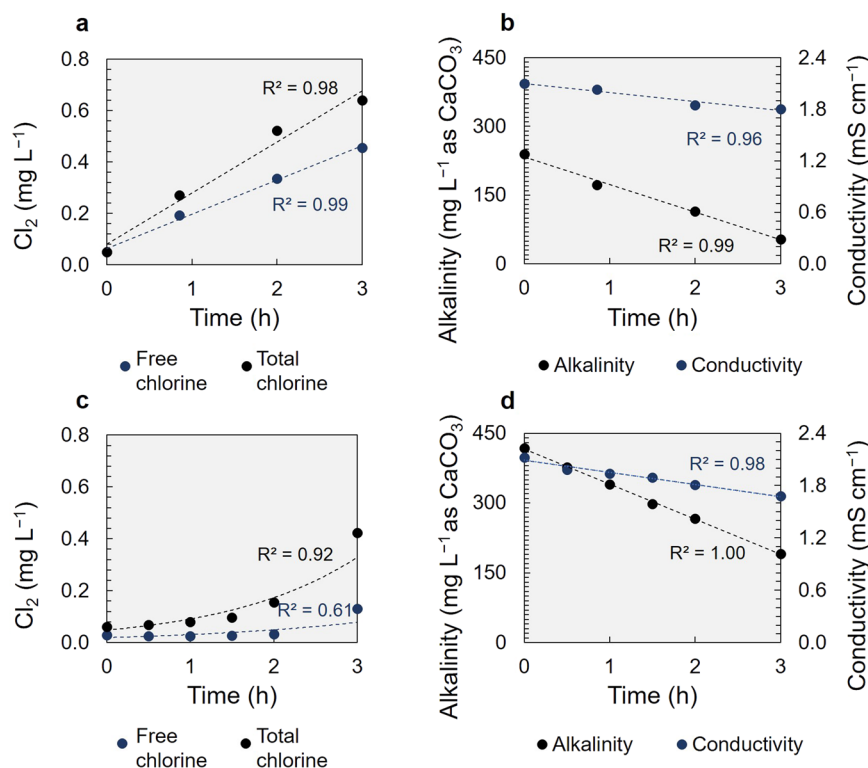
Fig. 3 Synthetic (SGW) vs real groundwater (GW-Cycle III P-FBR effluent) electrochlorination at 50 mA current ($j = 2$ mA cm^{-2} current density). a SGW chlorine, **b** SGW alkalinity and conductivity, **c** GW chlorine and **d** GW alkalinity and conductivity. The error bars represent the standard deviation of $n = 3$ analytical replicates.

Electrochemical disinfection of denitrified groundwater and the residual chlorine effect

The disinfection efficiency was further investigated in the presence of TC with the P-FBR GW-Cycles II and III effluents during electrolysis at 50, 100 and 150 mA ($j = 2$ mA cm^{-2}, 4 mA cm^{-2} and 6 mA cm^{-2}) (Fig. 4). To assess the impact of residual free chlorine, the TC load was measured in the disinfected water 24 hours after the completion of electrolysis.

At 2 mA cm^{-2} and with GW-Cycle II effluent, the free and total chlorine produced within 1 h were 0.049 (±0.002) mg L^{-1} and 0.109 (±0.001) mg L^{-1}, respectively, and the final pH was 7.07. During this run the TC load decreased by 1.01 log to a final 3.12 log MPN 100 mL^{-1} (Fig. 4a). In the run with GW-Cycle III effluent, completed in 3 h, the TC counts were eliminated already in 2 h of applied electrolysis time, achieving a 3.79 log removal of TC (Fig. 4a) when the free and total chlorine were 0.032 (±0.003) mg L^{-1} and 0.155 (±0.002) mg L^{-1}, respectively. At the completion of this test, $t = 3$ h, the final free and total chlorine concentrations were 0.132 (±0.001) mg L^{-1} and 0.423 (±0.003) mg L^{-1}, respectively and the final pH 6.84. At that time the cell was left in open circuit and the residual chlorine effect was demonstrated after 24 h. No TC could be detected in the disinfected groundwater (Fig. 4a).

At 4 mA cm^{-2}, the TC load was eliminated within 1 h in both GW-Cycle II and III, with 4.24 and 3.22 log removal for GW-Cycle II and III, respectively (Fig. 4b). The measured free and total chlorine varied in this case between the two cycles, with final 0.265 (±0.000) mg L^{-1} and 0.059 (±0.004) mg L^{-1} free chlorine concentration and 0.449 (±0.001) mg L^{-1} and 0.261 (±0.004) mg L^{-1} total chlorine concentration for GW-Cycle II and III, respectively. The final pH was 6.84 and 7.03 in GW-Cycle II and III.

At 6 mA cm^{-2} GW-Cycle II effluent, a 0.9 log TC removal was achieved within 30 min electrolysis time with a final 3.27 log MPN 100 mL^{-1} TC concentration, while for GW-Cycle III, the TC load decreased by 2.15 log, obtaining a treated groundwater with a

0.67 log MPN 100 mL^{-1} TC load (Fig. 4c). The measured free and total chlorine varied as well in this case between the two cycles, with 0.197 (±0.003) mg L^{-1} and 0.036 (±0.002) mg L^{-1} final free chlorine and 0.273 (±0.003) mg L^{-1} and 0.150 (±0.005) mg/L total chlorine concentrations for GW-Cycle II and III, respectively. These differences in chlorine concentration measurements between cycles II and III could have been resulting from differences in the local mixing conditions or differences in organics or metals present in the GW-Cycle III effluent that could interfere with the chlorine analysis. While the TC counts at 6 mA cm^{-2} GW-Cycle III were not completely eliminated within the electrolysis time, no TC were detected after 24 h.

The effect of charge density on energy consumption and disinfection

Two charge densities, 41.7 and 83.3 A h m^{-3}, were selected to investigate the impact of increasing charge density on chlorine production and disinfection efficacy. Additionally, the specific energy consumption of the electrochemical treatment was assessed. Both free and total chlorine increased with the charge density (Fig. 5a), however, the difference in the two concentrations obtained was not statistically significant. Considering that the denitrified groundwater is an impure electrolyte, differences in the TOC, the microbial load or even background color can induce variations in the production and measurement of Cl$_2$. Thus, it is important to exercise caution when comparing the two charge densities in terms of free chlorine production with denitrified groundwater, or in general polluted water, as the electrolyte.

A lower charge density and a lower chlorine concentration were already sufficient for complete TC elimination (Fig. 5b). More specifically, a 0.97 (±0.03) ratio of log TC decrease over the initial log TC counts was achieved with 41.7 A h m^{-3} and 0.043 (±0.009) mg L^{-1} free chlorine. Complete elimination of the TC counts was achieved with 83.3 A h m^{-3} and 0.115 (±0.099) mg L^{-1}
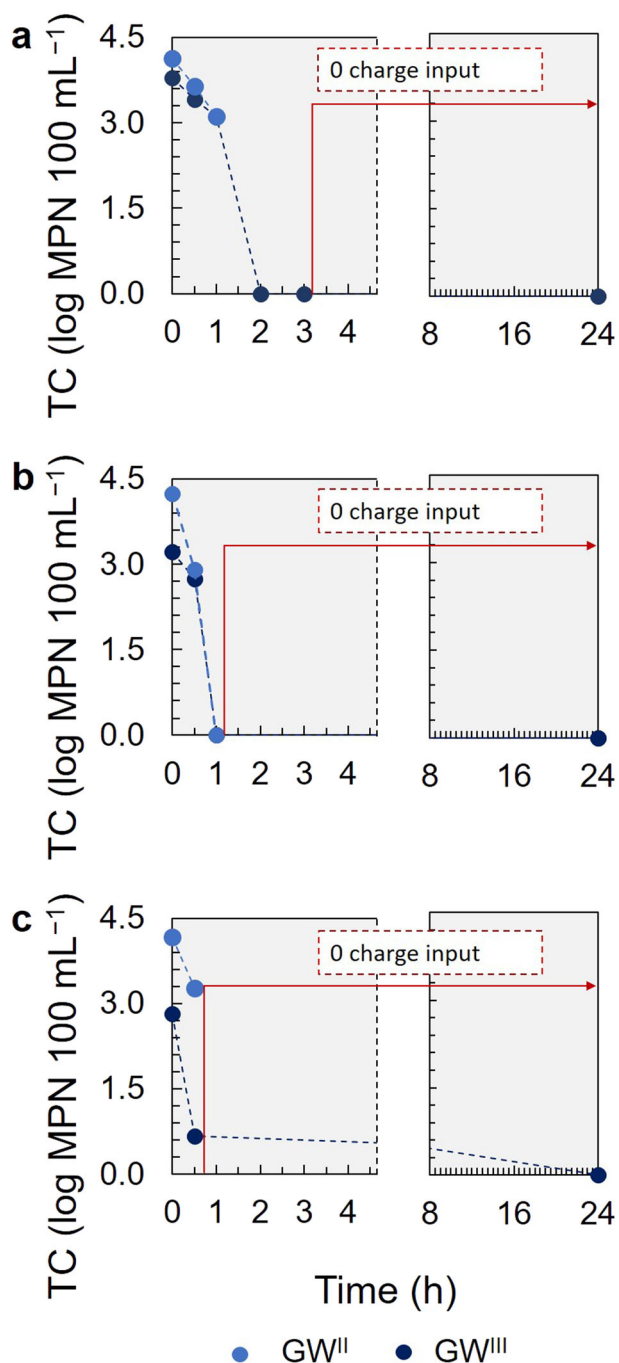
Fig. 4 **Disinfection of real groundwater (GW) at 50, 100 and 150 mA applied current (*j* = 2 mA cm^{-2}, 4 mA cm^{-2} and 6 mA cm^{-2}).** **a**: 50 mA, **b**: 100 mA and **c**: 150 mA, in two replicates, conducted with the P-FBR GW-Cycle II (light blue circles) and GW-Cycle III (dark blue circles) effluents, respectively. The residual effect of free chlorine is demonstrated at 24 h TC counts.

Fig. 5 **Charge density effect on the efficiency of disinfection and on the energy consumption. a** Chlorine (free and total) production (in mg L^{-1}), **b** total coliforms (TC) removal expressed as the ratio of log TC removal and initial TC log concentration ((log MPN 100 mL^{-1})/(log MPN 100 mL^{-1})) and **c** specific energy consumption for water treatment (SEC$_W$ in (kW h m^{-3}) for synthetic (SGW) and real groundwater from Cycles II and III (GW_II + III) at 41.7 and 83.3 (A h m^{-3}) charge density. The error bars represent the standard deviation of *n* = 3 experimental runs with GW-Cycle II and III and *n* = 4 experimental runs with SGW.

final free chlorine (Fig. 5a, b). Consistently lower values of free and total chlorine were measured with the GW compared to the SGW. Therefore, for a fair comparison, the free chlorine produced with SGW was 0.169 (±0.037) mg L^{-1} and 0.245 (±0.065) mg L^{-1} with 41.7 A h m^{-3} and 83.3 A h m^{-3}, respectively, while the total chlorine for the same charge densities was 0.300 (±0.006) mg L^{-1} and 0.471 (±0.121) mg L^{-1}, respectively (Supplementary Table 3).

The specific energy consumption (SEC$_W$) for the disinfection of the denitrified groundwater increased with increasing charge
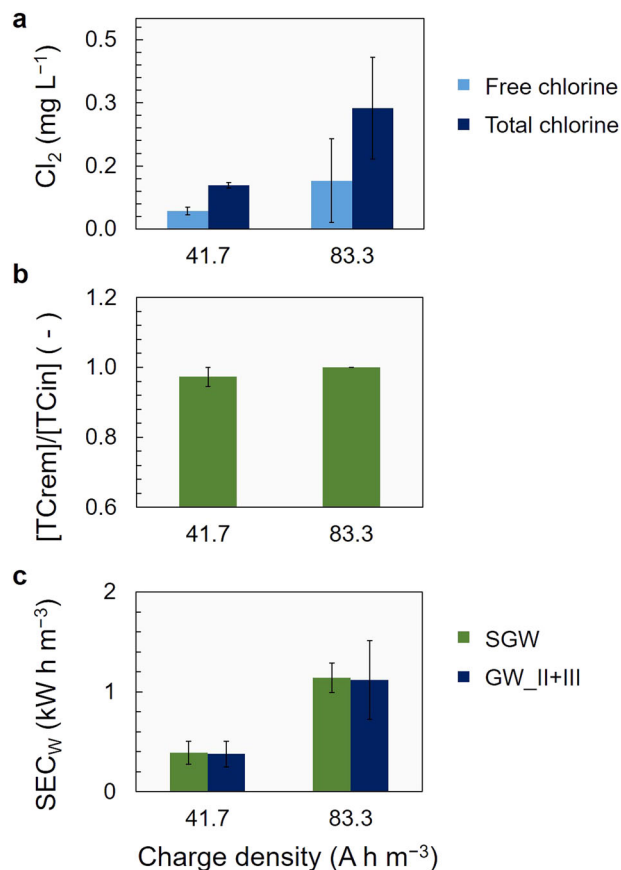
density, both for SGW and GW (Fig. 5c). The SEC$_W$ was ~0.4 and ~1.1 kW h m^{-3} for both SGW and GW at 41.7 and 83.3 A h m^{-3}, respectively, and the similarity can be attributed to the similar conductivities of the two solutions (~2 mS cm^{-1}). At 41.7 A h m^{-3}, the cell voltage with SGW was 10.9 (±1.7) V and with GW, 9.1 (±3.1) V. At 83.3 A h m^{-3} the cell voltage obtained was 13.7 (±1.8) V and 13.4 (±4.7) V, respectively.

DISCUSSION

The average denitrification rate obtained by the P-FBR was 171 mg NO$_3^-$ L^{-1} d^{-1} at 22 (±2) °C, 1 to 2 orders of magnitude higher than the rates obtained in bottle studies on FeS$_2$-based groundwater denitrification[18,19]. To date, the majority of research on auto-trophic FeS$_2$ denitrification has been carried out at around 30 °C, as this temperature range is expected to facilitate higher denitrification activity. The effect of temperature on the deni-trification efficiency was studied by Xu et al.[32], who demonstrated that a drop of temperature from 28 to 20 °C resulted in a 48% decrease in the denitrification efficiency, while it also contributed to an increase in the effluent NO$_2^-$ concentration. One of the few studies conducted at 20 °C was the study of Tong et al.[33], where a 56.4% NO$_3^-$ removal efficiency was achieved, with a similar sized

column as in the present study, however with a three times higher FeS_2 mass.

In our study, low effluent SO_4^{2-} concentration was obtained, 28 mg L^{-1} in average for all three cycles with real groundwater (Table 1), with a marginal increase of the SO_4^{2-} concentration from the influent to the effluent of the P-FBR (Table 1 and Supplementary Table 1). An increase in SO_4^{2-} as a product of FeS_2-based denitrification is expected, however, the produced SO_4^{2-} was well below the expected stoichiometric amount based on the NO_3^- removal. Consistently lower SO_4^{2-} concentrations than the stoichiometrically expected have been reported in FeS_2 denitrification studies, without providing conclusive, quantitative evidence[33–35]. Although the low SO_4^{2-} effluent concentrations obtained seem advantageous for water reuse schemes, longer-term experiments and a more detailed examination of the denitrification products and the precipitates formed in FeS_2-based denitrification reactors will be required to conclude on this described advantage of FeS_2 over other sulfurous electron donors[33].

Furthermore, a marginally higher K^+ concentration was observed in the effluent of the denitrifying reactor in our study that was consistent in all three cycles with GW and cannot be attributed to any specific reactions describing FeS_2 denitrification. It can be hypothesized that the K^+ measured in the effluent originated from the FeS_2 as an impurity and was subsequently released after FeS_2 utilization. In a study conducted on FeS_2 aerobic bioleaching the initial FeS_2 used contained K, while the neutralizing agent not. The elemental composition of the bioleach liquor consistently showed a K concentration higher than 1% after pyrite biooxidation[36]. While this suggests the possibility of K^+ leaching following FeS_2 biooxidation, there is no conclusive evidence to support the hypothesis that the higher K^+ levels in our effluent are a result of this process, particularly since the experimental conditions in that study, specifically the pH and oxidative conditions, were different from those in our experiments. Moreover, we did not conduct a FeS_2 compositional analysis. Hence, the hypothesis that K^+ in the effluent originated from the impurities present in FeS_2 deserves further scrutiny. In conclusion, it is crucial to thoroughly examine the composition of FeS_2 before use, particularly in water reuse schemes.

The ability of bacterial cells to use FeS_2, a solid electron donor, for denitrification has been demonstrated in nature, yet the exact mechanism of the FeS_2 utilization is still being debated[10]. Direct FeS_2 utilization or indirect, through FeS_2 dissolution mechanisms, have been proposed. However, it is difficult to determine which is the most probable route and to distinguish between the two[10,37]. The high denitrification rates obtained in this study could be partially attributed to the active denitrifying mixed community present in the biomass that was used to inoculate the P-FBR, which was obtained from the study of Carboni et al.[17]. Furthermore, between batch and continuous operation (day 8) the O_2 content of the headspace increased from between 2 to 3% up to 10% due to an operational upset (Supplementary Fig. 2a). This resulted in a measurable increase in the Fe^{2+} and $S_2O_3^{2-}$ concentrations in the reactor (Supplementary Figs. 2a and 2b), which could be linked to FeS_2 dissolution[10]. After this upset, denitrification rates as high as 400 mg NO_3^- L^{-1} d^{-1} were observed, around ten times higher than in the first batch operation and the subsequent continuous operation. Previous research on FeS_2 autotrophic denitrification has suggested that FeS_2 dissolution might be an essential step prior to its utilization for denitrification[15,38–40]. This suggests that the previously mentioned mechanism may have occurred in the reactor.

However, these results are rather limited to allow for commentary on the exact mechanism of FeS_2 obtained in the studied reactor during the total course of the experimental period. Surface and composition analysis of the FeS_2 before and after operation could reveal changes in the morphology of the FeS_2 and

give an indication of the parts of FeS_2 utilized by the microbial community for denitrification[37]. Studies that combine microbial community analysis with surface analysis in controlled media are essential in deciphering the FeS_2-driven denitrification mechanisms. The latter will also allow for future optimization of FeS_2 autotrophic denitrification systems and for establishment of these systems in the water treatment lines.

Chlorine production was achieved with a Pt/Ti anode and efficiently disinfected the denitrified SGW and GW effluents (Fig. 3). In electrochlorination studies, electrodes employing expensive, mixed metal oxide (MMO) coatings[27,41,42] or boron-doped diamond (BDD)[28] electrodes have been extensively tested, as they are more robust and demonstrate higher oxidation rates. More specifically, Ru MMO demonstrates a higher affinity towards Cl_2 evolution[23,43], compared to O_2 evolution, two reactions that occur at similar electrode potentials[24,25]. In this study, a custom-made Pt/Ti electrode with a Ti current collector laser welded perpendicularly to the electrode surface was used as an anode and supported complete disinfection of real GW (Fig. 4 and Supplementary Fig. 3c).

At 41.7 A h m^{-3} a 3.8 log removal of TC was achieved corresponding to a 0.4 kW h m^{-3} SECw, when the free chlorine measured was in average 0.043 mg L^{-1} with GW and 0.169 mg L^{-1} with SGW. Patermarakis and Fountoukidis[44] in one of the first studies on electrochlorination with a low-cost Ti electrode achieved in average a 5-log removal of germs, without specifying the type, with 89.3 A h m^{-3} charge investment, resulting in 4 kW h m^{-3} SECw. A Pt/Ti anode was also used in the study of Qing et al.[30] that reduced the microbial content of irrigation water by 5 log with 9 A h m^{-3} charge investment and achieved a three times higher free chlorine concentration, even though the initial Cl^- concentration was as low as 1.85 mg/L. In their study to treat microbially contaminated groundwater, De Battisti et al.[28] used a BDD electrode that eliminated the 200 MPN 100 mL^{-1} TC and E. coli load with a 28 A h m^{-3} charge density, however, no results were reported on the cell voltage obtained to allow for SECw calculations. Disinfection was evaluated in our study using total coliforms (Fig. 4). However, more persistent pathogens, including viral species, might require higher doses of chlorine and longer contact times. Thus, further research on electrochlorination times and power investment for those microbial contaminants should be conducted[28,45,46].

The production rates for both free and total chlorine with SGW remained stable between the first and the second hour of operation, while they dropped in the last hour (Fig. 3). Several processes could be responsible for this reduced Cl_2 production rate in our system. For instance O_2 bubble formation, which was apparent in our experiments, obstructing the electrolyte-electrode contact and thus limiting the Cl^- oxidation rate, electrode surface modifications induced by oxidation reactions, or further, free chlorine inorganic by-products formation[25,44,47]. Without specific analysis of all the chlorination products produced, the pH changes in the electrolyte and without electrode surface analysis before and after the experimental cycles, it is difficult to identify which specific process, or combination of processes, is responsible for the observed effects.

Regardless of the mechanism that led to the reduction of chlorination rates in the last hour of the experiment, what is most important in the case of disinfection is maintaining consistency and a stable voltage to ensure effective treatment. One way to achieve this may be through reverse polarity[30,44]. To ensure long-term operational stability of the electrodes for disinfection, further testing is required. Additionally, careful examination of the by-products resulting from Cl_2 disinfection is necessary when considering water reuse. Prioritizing these factors is essential to ensure that the proposed disinfection processes will be effective and sustainable in the long term.

The P-FBR was operated for 100 days in total at ambient 22 (±2) ℃ temperature, with a consistent 79% NO_3^- removal efficiency to achieve the potable water limit of $NO_3^- < 50$ mg L^{-1}. Additionally, the denitrified effluent was disinfected electrochemically with 41.7 A h m^{-3} charge density and 0.4 kW h m^{-3} energy consumption. The combined treatment was realized without additional input of vitamins, or chemicals for pH control. The electrochemical cell operates solely on electricity, which can be generated from renewable sources such as solar or wind energy, which may allow location and electrical grid independency. Furthermore, the chlorination process takes place on-site, eliminating the need to purchase chemicals, as the Cl$^-$ required to initiate disinfection is naturally present in the groundwater. The electrochemical unit could further enhance denitrification by making use of the H$_2$ that is produced at the cathode. The H$_2$ can serve as an additional electron donor for autotrophic denitrification and improve the overall NO_3^- removal efficiency[48,49].

Pathogens in drinking water have been linked to water-borne diseases, such as cholera, typhoid and diarrhea. An indication of the severity of the problem is the recent cholera outbrakes in Sub-Saharan African countries[50]. Exposure to high concentrations of nitrate in drinking water has been linked with infant respiratory problems and several other health issues[51]. Furthermore, the high chemical usage and dependence of current water treatment methods are of significant concern, particularly for landlocked countries. Approaches that can limit chemical use and provide chemical independence, where possible, are urgently required. In this regard, the combination of autotrophic FeS$_2$-based denitrification with electrochemical disinfection could provide an inexpensive, renewable and small-footprint system for groundwater remediation, to comply with the SDG6.1.1 indicator for safe drinking water access that is free from fecal and chemical contamination, located on the premises and readily available.

METHODS

Media and groundwater

Experiments in the P-FBR and EC reactors were conducted with synthetic (SGW) and real (GW) groundwater that was supplemented with nitrate (as NaNO$_3$) (GW-Cycle I), chloride (as NaCl) (GW-Cycle II) and a higher concentration of total coliforms (TC) (GW-Cycle III) (Table 2). The SGW recipe was prepared according to the maximum values of previous studies with synthetic polluted

Table 2. Operational scheme of the pyrite-based fluidized bed reactor (P-FBR) treating synthetic (SGW) and real (GW) groundwater.

Operational periods	HRT [h]	Operational time [d]
Batch 1	—	0–5
3× Batch	—	5–23
SGW-Cycle I	24	23–33
SGW-Cycle II	12	33–46
SGW-Cycle III	18	46–64
GW-Cycle I	18	64–80
GW-Cycle II	18	80–89
GW-Cycle III	18	89–100

SGW Synthetic groundwater.
GW-Cycle I: real groundwater with NaNO$_3$ addition to final 178 mg NO$_3^-$ L^{-1} concentration.
GW-Cycle II: real groundwater with NaNO$_3$ and NaCl addition to final 178 mg NO$_3^-$ L^{-1} and 283 mg Cl$^-$ L^{-1} concentration.
GW-Cycle III: real groundwater with NaNO$_3$, NaCl and total coliforms addition to final 178 mg NO$_3^-$ L^{-1}, 283 mg Cl$^-$ L^{-1} and 500 MPN 100 mL^{-1} total coliforms concentration.

groundwater and real polluted groundwater[28,52,53] and contained: 0.005 g L^{-1} KNO$_3$, 0.24 g L^{-1} NaNO$_3$, 0.2 g L^{-1} MgSO$_4$·7H$_2$O, 0.043 g L^{-1} MgCl$_2$·6H$_2$O, 0.2 g L^{-1} CaCl$_2$, 0.01 g L^{-1} NH$_4$Cl, 0.1 g L^{-1} NaHCO$_3$, 0.22 g L^{-1} NaCl and 0.02 g L^{-1} FeSO$_4$·7H$_2$O (178 mg NO$_3^-$ L^{-1} and 283 mg Cl$^-$ L^{-1}) (Supplementary Table 4).

Groundwater was sampled from two different privately owned wells in Co. Clare and Co. Galway in Ireland (characteristics presented in Supplementary Table 5) and was fridge stored at 4 ℃ till use as influent in the P-FBR. Although the groundwater sampled was contaminated with pathogens (Supplementary Table 5), the NO$_3^-$ and Cl$^-$ concentrations were well below the concentrations that would be expected in a polluted groundwater source. Therefore, for subsequent experiments, real groundwater was used as the background solution and NO$_3^-$, Cl$^-$ and TC were added in the respective cycles (Table 2) to reach 178 mg NO$_3^-$ L^{-1}, 283 mg Cl$^-$ L^{-1} and 500 MPN 100 mL^{-1} total coliforms in GW-Cycles I, II and III (Table 2).

Pyrite-based denitrification experiments

The fluidized bed denitrifying reactor (P-FBR) was a 6.5 cm diameter, 1 L glass column, as described in Carboni et al.[17] (Fig. 6 and Supplementary Fig. 3a). The working liquid volume of the reactor, including recirculation piping, was 800 mL and the headspace was 200 mL. Two electrode probes were immersed in the liquid bed, for continuous monitoring of the ORP (MTC101, Hach®, Düsseldorf, Germany) and the pH (PHC101, Hach®, Düsseldorf, Germany) and were connected to portable HQ™ Series meters (Hach®, Düsseldorf, Germany). The headspace of the reactor was connected to a 1 L gas bag filled with 99.99% N$_2$ gas to maintain anaerobic conditions in the reactor, as well as to a liquid displacement column to monitor excess production of N$_2$ as the product of the denitrification process. A bed of approximately 10 cm was created at the bottom of the reactor by addition of 120 g FeS$_2$ (99+% grade, 0.15–0.48 cm diameter, from Fischer Scientific, Hampton, USA) as described in Carboni et al.[17]. Fluidization was achieved with continuous upflow liquid recirculation by a peristaltic pump (323 S/D Watson Marlow, UK) at 200 mL min^{-1} allowing for a 30% – 40% bed expansion. The temperature in the reactor was not controlled, but it was monitored externally with a thermometer and it was stable at 22 (±2) ℃.

Synthetic groundwater was used as medium and subsequent to the FeS$_2$ addition, the reactor was flushed with 99.99% N$_2$ through a gas bag to obtain anoxic conditions. Anoxic conditions were monitored with the ORP probe and were confirmed when the ORP dropped to values below 0 mV, as well as when the O$_2$% in the headspace dropped to 2%. The reactor was then inoculated with 20% of the working volume (approximately 160 mL) with inoculum consisting of 60 mL of FeS$_2$ biomass, directly obtained from a FeS$_2$ denitrifying FBR, as described in Carboni et al.[17] and 100 mL of the same biomass activated with S$_2$O$_3^{2-}$ as electron donor in prior bottle incubations (data not shown). Initially, the reactor was operated in batch and after obtaining denitrification the reactor was switched to continuous operation, whereby the medium was supplied continuously from a 10 L bottle stored at 4 ℃, with a peristaltic pump (Masterflex Cole-Parmer, Chicago, USA) according to the HRT required in every cycle (Table 2).

The denitrification performance of the P-FBR was evaluated based on the nitrate removal rate (in mg L^{-1} d^{-1}, calculated as:

$$\text{Nitrate removal rate} = \frac{[NO_3^-]_{eff} - [NO_3^-]_{inf}}{\frac{HRT}{24}} \quad (1)$$

where $[NO_3^-]_{eff}$ and $[NO_3^-]_{inf}$ are the effluent and influent concentrations of nitrate (in mg L^{-1}) and HRT (in h) is the hydraulic retention time, that was 24, 12 and 18 h for the synthetic GW (SGW) experimental periods and 18 h for the experimental periods with the real groundwater (GW) (Table 2).
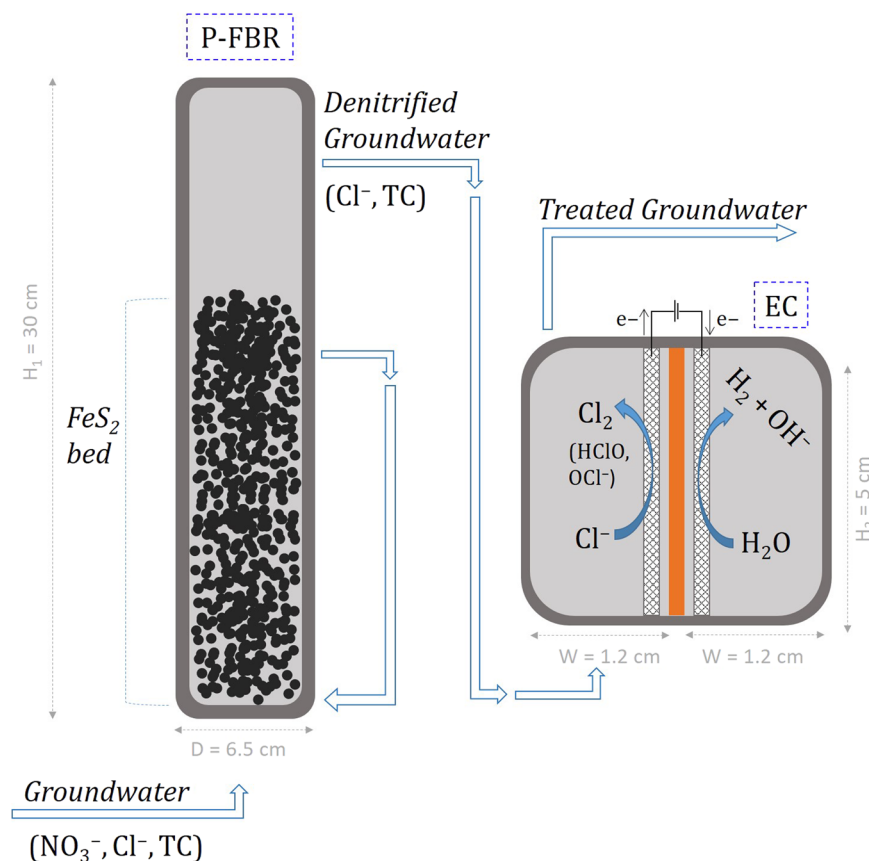
Fig. 6 Schematic drawing of the combined pyrite-based denitrification reactor (P-FBR) and electrochlorination (EC) reactor for nitrate (NO_3^-) and total coliforms (TC) removal from groundwater (set-up picture in Supplementary Fig. 3). H_1 and D are the height and the diameter of the P-FBR and H_2 and W are the internal height and width of each of the two electrode chambers separated by the cation exchange membrane.

Electrochemical disinfection experiments

All electrochemical experiments were conducted with a two compartment electrochemical cell (internal dimensions: $5 \times 5 \times 1.2$ cm) allowing for an internal volume of 30 mL for each electrode compartment (Supplementary Fig. 3b). The inner and outer frames of the electrochemical cell were constructed from 4 PMMA transparent acrylic sheets with 1.2 cm thickness (Good-fellow, Hamburg, Germany). The two compartments were separated by a cation exchange membrane (CEM) (Fumasep© FKL-PK-130, Fumatech GmbH, Germany). Two platinum coated titanium (Pt/Ti) planar meshes (Redoxme AB, Norrköping, Sweden) with 5×5 cm projected surface were used as anode and cathode and two Ti rods (D = 3 mm) (Goodfellow, Hamburg, Germany) were used as current collectors. The Ti rods were laser welded under argon (Ar) gas shielding, perpendicular to the electrode surface (conducted by Dawnlough Ltd., Galway, Ireland) (Supplementary Fig. 3c). The two electrodes were positioned parallel to each other (distance between electrodes was ~5 mm). A 3 M KCl Ag/AgCl electrode (BASi MF-2056, BASi, IN, USA, +0.210 V vs. SHE at 25 °C) was used as reference electrode (RE) in the anodic compartment and all reported potentials refer to this electrode. The electrochemical cell was controlled galvanostatically with a DC power supply (RS PRO Bench Power Supply, 150 W, 1 Output, $0 \to 30$ V, $0 \to 5$ A, RS Radionics, Dublin, Ireland) and electroche-mical techniques were performed with a VSP potentiostat (Bio-Logic Science Instruments SAS, Seysinnet-Pariset, France). All current densities are reported with respect to the projected surface area of the anode (25 cm²).

Prior to cell operation, the compensated resistance between the anode and the reference electrode (R_{an}, 80% compensation by potentiostat) and the cell resistance (R_{cell}) were measured with the current interrupt (CI) method[54] in 10 successive cycles (cycles of 50 ms at 100 mA followed by 50 ms open circuit with a recording period of 0.2 ms). The electrolyte used was SGW and GW according to the cycle that was tested every time and the resistances measured were 0.07 (±0.03) Ω for the anode and 17.83 (±3.83) Ω across the cell. The anode potential (E_{WE}) and cell voltage (E_{cell}) were monitored with the potentiostat by chronopotentiometry (CP).

The effluent of the denitrification reactor was treated in batch (1.2 L, total effluent of one day) in the anodic compartment of the electrochemical reactor, with an electrolysis time of 30, 60, 120, 180 min, depending on the current applied. In every batch test, the respective effluent of the P-FBR was used as anolyte (Table 3), while a 8.3 mM NaOH solution was used as catholyte (EC $\approx$ 2 mS cm⁻¹), similar to the anolyte). Anolyte and catholyte were recirculated through the electrode compartments from 2 L bottles with a peristaltic pump (323 S/D Watson Marlow, Falmouth, UK) at 75 rpm. Samples for all chemical analyses were taken from the anolyte and catholyte recirculation lines.

The charge density (in A h m⁻³) was calculated as:

$$\text{Charge density} = \frac{I \times t_{electrolysis}}{V_{anolyte} \times 60} \qquad (2)$$

where I is the constant current applied (in mA), which was 50, 100 and 150 mA for the respective 2, 4 and 6 mA cm⁻² current densities tested, $t_{electrolysis}$ is the time of electrolysis batch (in min) and $V_{anolyte}$ is the volume of the anolyte in every batch, which was 1.2 L.

Table 3. Operational scheme of the electrochemical reactor treating synthetic (SGW) and real (GW) P-FBR effluent.

Anolyte solution	Current applied [mA]	Replicates
SGW	50	3
	100	2
	150	1
GW-Cycle I	50	1
GW-Cycle II	50	1
	100	1
	150	1
GW-Cycle III	50	1
	100	1
	150	1

The specific energy consumption (SECw in (kW h m^{-3}) for the treatment of denitrified groundwater was calculated as:

$$SECw = charge\ density \times E_{cell} \qquad (3)$$

where E_{cell} is the cell voltage (in V), that was monitored during electrolysis.

Analytical methods

Liquid samples taken from the influent and effluent of the P-FBR, as well as from the anolyte and catholyte of the electrochemical cell were filtered through a 0.22 μm membrane filter and were analyzed for NO_2^-, NO_3^-, SO_4^{2-}, $S_2O_3^{2-}$, Cl^- and PO_4^{3-} with a Dionex Aquion Ion Chromatography System (ThermoFisher Scientific, Waltham, USA), equipped with an IonPac AS14 A 4×250 mm column coupled to a AG14 A 4×50 mm guard column, running with a 3.03 mM $NaHCO_3$/ 0.97 mM Na_2CO_3 eluent at 1 mL min^{-1} flow rate[55]. Total iron (Fe), K^+, Na^+, Mg^{2+} and Ca^{2+} were analyzed with an ICP-OES (ThermoFisher, Scientific Walthan, USA) operated at RF power: 1.2 kW, Ar plasma flow rate: 12 L min^{-1}, auxiliary Ar flow rate: 1 L min^{-1} and nebulizer argon flow rate: 0.7 L min^{-1}[17]. Ferrous iron (Fe^{2+}), NH_4^+ (ppm) and alkalinity (mg L^{-1} as CaCO$_3$) were measured with the colorimetric methods SM: 3500 Fe-B: Iron by Phenanthroline[56], EPA-NERL: 350.1: (Rev. 2.0 1993): Ammonia by automated colorimetry[57] and EPA 310.2 (Rev. 1974): Alkalinity by autoanalyser[58], respectively, and analyzed photometrically with a Thermo Scientific™ Gallery™ automated analyzer (Thermo Fisher Scientific Oy, Vantaa, Finland), according to the manufacturer's protocols. Ferric iron (Fe^{3+}) concentrations were calculated as the difference between the measured Fe and Fe^{2+} concentrations. Electrical conductivity (EC) and pH were analyzed electrochemically with a Thermo Scientific™ Gallery™ analyzer equipped with a Gallery ECM unit with functional pH (984997) and reference electrodes (984996) (Thermo Fisher Scientific Oy, Vantaa, Finland), according to the manufacturer's protocols.

Total carbon (TC) and inorganic carbon (IC) concentrations were measured with a TOC analyzer (TOC-L, Shimadzu, Kyoto, Japan) and the difference of the two was calculated as total organic carbon (TOC)[17]. Total nitrogen (TN) was determined photometrically with a SEAL Autoanalyzer AA3 3HR (SEAL Analytical Ltd, Wrexham, UK), according to Method No. G-157-96 Rev. 17 (Multitest MT17) (Hydrazine method) provided by the manufacturer. Gas samples taken from the headspace of the P-FBR were analyzed with a gas chromatograph (7890B, Agilent, Santa Clara, USA), equipped with a mass spectrometer (GC-MS) heated at 250 °C. Helium was used as the carrier gas with a flow rate of 2.5 mL min^{-1}[17].

Chlorine analysis

Samples for free and total chlorine analysis were taken from the anolyte and catholyte recirculation lines and were measured immediately with a UV-1900 spectrophotometer with a temperature control chamber (Shimadzu, Kyoto, Japan) according to the standard DPD Colorimetric Method (4500 – Cl G)[59]. The resulting intensity was related to chlorine concentrations by means of a calibration curve (0.05–4 mg Cl$_2$ L^{-1}) constructed initially at 515 nm with KMnO$_4$ standard solutions.

Detection of total coliforms (TC) and *E. coli*

The Most Probable Number (MPN) of TC and *E. coli* was determined by the quanti-tray/2000 Colilert-18® test (9223 B-2004 Colilert-18®)[60] in 100 mL (MPN 100 mL^{-1}) samples taken from the P-FBR influent and effluent as well as from the anolyte of the electrochemical cell. An IDEXX Quanti-tray sealer (IDEXX Laboratories Inc., Maine, USA) was used to seal the trays that were subsequently incubated for 22 h at 35 °C. For all dilutions required, filtered sterilized distilled water was used.

REFERENCES

1. Lapworth, D. J. et al. Urban groundwater quality in sub-Saharan Africa: current status and implications for water security and public health. *Hydrogeol. J.* **25**, 1093–1116 (2017).
2. Carrard, N., Foster, T. & Willetts, J. Groundwater as a source of drinking water in southeast Asia and the Pacific: A multi-country review of current reliance and resource concerns. *Water* **11**, 1605 (2019).
3. Baily, A., Rock, L., Watson, C. J. & Fenton, O. Spatial and temporal variations in groundwater nitrate at an intensive dairy farm in South-East Ireland: Insights from stable isotope data. *Agric. Ecosyst. Environ.* **144**, 308–318 (2011).
4. Reaver, K. M. et al. Drinking water quality and provision in six low-income, peri-urban communities of Lusaka, Zambia. *GeoHealth* **5**, e2020GH000283 (2021).
5. Masindi, V. & Foteinis, S. Groundwater contamination in sub-Saharan Africa: Implications for groundwater protection in developing countries. *Clean. Eng. Technol.* **2**, 100038 (2021).
6. Ravikumar, P., Venkatesharaju, K. & Somashekar, R. K. Major ion chemistry and hydrochemical studies of groundwater of Bangalore South Taluk, India. *Environ. Monit. Assess.* **163**, 643–653 (2010).
7. *Guidelines for drinking-water quality - Fourth edition incorporating the first and second addenda. Licence: CC BY-NC-SA 3.0 IGO* (World Health Organization, 2011).
8. Pang, Y. & Wang, J. Various electron donors for biological nitrate removal: a review. *Sci. Total Environ.* **794**, 148699 (2021).
9. Di Capua, F., Pirozzi, F., Lens, P. N. L. & Esposito, G. Electron donors for autotrophic denitrification. *Chem. Eng. J.* **362**, 922–937 (2019).
10. Hu, Y., Wu, G., Li, R., Xiao, L. & Zhan, X. Iron sulphides mediated autotrophic denitrification: an emerging bioprocess for nitrate pollution mitigation and sustainable wastewater treatment. *Water Res.* **179**, 115914 (2020).
11. Jørgensen, C. J., Jacobsen, O. S., Elberling, B. & Aamand, J. Microbial oxidation of pyrite coupled to nitrate reduction in anoxic groundwater sediment. *Environ. Sci. Technol.* **43**, 4851–4857 (2009).
12. Zhang, Y. C., Slomp, C. P., Broers, H. P., Passier, H. F. & Van Cappellen, P. Denitrification coupled to pyrite oxidation and changes in groundwater quality in a shallow sandy aquifer. *Geochim. Cosmochim. Acta* **73**, 6716–6726 (2009).
13. Schwientek, M. et al. Evidence for denitrification regulated by pyrite oxidation in a heterogeneous porous groundwater system. *Chem. Geol.* **255**, 60–67 (2008).
14. Hayakawa, A., Hatakeyama, M., Asano, R., Ishikawa, Y. & Hidaka, S. Nitrate reduction coupled with pyrite oxidation in the surface sediments of a sulfide-rich ecosystem. *J. Geophys. Res. Biogeosci.* **118**, 639–649 (2013).

15. Pang, Y. & Wang, J. Insight into the mechanism of chemoautotrophic denitrification using pyrite (FeS_2) as electron donor. *Bioresour. Technol.* **318**, 124105 (2020).

16. Kong, Z., Li, L., Feng, C., Dong, S. & Chen, N. Comparative investigation on integrated vertical-flow biofilters applying sulfur-based and pyrite-based autotrophic denitrification for domestic wastewater treatment. *Bioresour. Technol.* **211**, 125–135 (2016).

17. Carboni, M. F. et al. Autotrophic denitrification of nitrate rich wastewater in fluidized bed reactors using pyrite and elemental sulfur as electron donors. *Environ. Technol. Innov.* **28**, 102878 (2022).

18. Pu, J. et al. Pyrite-based autotrophic denitrification for remediation of nitrate contaminated groundwater. *Bioresour. Technol.* **173**, 117–123 (2015).

19. Torrentó, C., Cama, J., Urmeneta, J., Otero, N. & Soler, A. Denitrification of groundwater with pyrite and Thiobacillus denitrificans. *Chem. Geol.* **278**, 80–91 (2010).

20. Mao, J. et al. Resource utilization of waste tailings: Simulated removal of nitrogen from secondary effluent by autotrophic denitrification based on pyrite tailings. *Front. Environ. Sci.* **10**, 1–9 (2022).

21. Botti, A. et al. Electrifying secondary settlers to enhance nitrogen and pathogens removals. *Chem. Eng. J.* **451**, 138949 (2023).

22. Hand, S. & Cusick, R. D. Electrochemical disinfection in water and wastewater treatment: identifying impacts of water quality and operating conditions on performance. *Environ. Sci. Technol.* **55**, 3470–3482 (2021).

23. Kraft, A. Electrochemical water disinfection: a short review. *Platin. Met. Rev.* **52**, 177–185 (2008).

24. Du, J., Chen, Z., Chen, C. & Meyer, T. J. A half-reaction alternative to water oxidation: chloride oxidation to chlorine catalyzed by silver ion. *J. Am. Chem. Soc.* **137**, 3193–3196 (2015).

25. Vos, J. G. & Koper, M. T. M. Measurement of competition between oxygen evolution and chlorine evolution using rotating ring-disk electrode voltammetry. *J. Electroanal. Chem.* **819**, 260–268 (2018).

26. Wang, L. et al. Hypochlorous acid as a potential wound care agent: part I. Stabilized hypochlorous acid: a component of the inorganic armamentarium of innate immunity. *J. Burns Wounds* **6**, e5 (2007).

27. Mosquera-Romero, S. et al. Disinfection of constructed wetland effluent by: In situ electrochemical chlorine production for water reuse. *Environ. Sci. Water Res. Technol.* **8**, 98–107 (2022).

28. De Battisti, A., Formaglio, P., Ferro, S., Al Aukidy, M. & Verlicchi, P. Electrochemical disinfection of groundwater for civil use – an example of an effective endogenous advanced oxidation process. *Chemosphere* **207**, 101–109 (2018).

29. Bhattacharya, M., Bandyopadhyay, K. & Gupta, A. Design of a cost-effective electrochlorination system for point-of-use water treatment. *Environ. Eng. Res.* **26**, 0–1 (2021).

30. Qing, G. et al. Disinfection of irrigation water using titanium electrodes. *J. Electrochem. Soc.* **168**, 63502 (2021).

31. Castellar, J. A. C. et al. Nature-based solutions coupled with advanced technologies: an opportunity for decentralized water reuse in cities. *J. Clean. Prod.* **340**, 130660 (2022).

32. Xu, B., Shi, L., Zhong, H. & Wang, K. The performance of pyrite-based autotrophic denitrification column for permeable reactive barrier under natural environment. *Bioresour. Technol.* **290**, 121763 (2019).

33. Tong, S., Rodriguez-Gonzalez, L. C., Feng, C. & Ergas, S. J. Comparison of particulate pyrite autotrophic denitrification (PPAD) and sulfur oxidizing denitrification (SOD) for treatment of nitrified wastewater. *Water Sci. Technol.* **75**, 239–246 (2017).

34. Di Capua, F., Mascolo, M. C., Pirozzi, F. & Esposito, G. Simultaneous denitrification, phosphorus recovery and low sulfate production in a recirculated pyrite-packed biofilter (RPPB). *Chemosphere* **255**, 126977 (2020).

35. Carboni, M. F., Arriaga, S. & Lens, P. N. L. Simultaneous nitrification and autotrophic denitrification in fluidized bed reactors using pyrite and elemental sulfur as electron donors. *Water Sci. Eng.* **16**, 143–153 (2023).

36. Gahan, C. S., Sundkvist, J. E. & Sandström, Å. A study on the toxic effects of chloride on the biooxidation efficiency of pyrite. *J. Hazard. Mater.* **172**, 1273–1281 (2009).

37. Dong, B., Jia, Y., Tan, Q., Sun, H. & Ruan, R. Contributions of microbial 'contact leaching' to pyrite oxidation under different controlled redox potentials. *Minerals* **10**, 1–16 (2020).

38. Liu, T., Hu, Y., Chen, N., He, Q. & Feng, C. High redox potential promotes oxidation of pyrite under neutral conditions: Implications for optimizing pyrite autotrophic denitrification. *J. Hazard. Mater.* **416**, 125844 (2021).

39. Dos Santos, E. C., De Mendonça Silva, J. C. & Duarte, H. A. Pyrite oxidation mechanism by oxygen in aqueous medium. *J. Phys. Chem. C* **120**, 2760–2768 (2016).

40. Yan, R., Kappler, A. & Peiffer, S. Interference of nitrite with pyrite under acidic conditions: implications for studies of chemolithotrophic denitrification. *Environ. Sci. Technol.* **49**, 11403–11410 (2015).

41. Annamalai, S., Futalan, C. C. & Ahn, Y. Electrochemical disinfection of simulated ballast water using RuO_2-TiO_2/Ti electrode. *Int. J. Environ. Res. Public Health* **19**, 1–11 (2022).

42. Talekar, G. V. et al. Sanitation of blackwater via sequential wetland and electrochemical treatment. *npj Clean. Water* **1**, 1–9 (2018).

43. Jeong, J., Kim, C. & Yoon, J. The effect of electrode material on the generation of oxidants and microbial inactivation in the electrochemical disinfection processes. *Water Res.* **43**, 895–901 (2009).

44. Patermarakis, G. & Fountoukidis, E. Disinfection of water by electrochemical treatment. *Water Res.* **24**, 1491–1496 (1990).

45. Bicudo, B., Van Der Werff, B., Medema, G. & Van Halem, D. Disinfection during iron electrocoagulation: differentiating between inactivation and floc entrapment for *Escherichia coli* and Somatic Coliphage ØX174. *ACS EST Water* **2**, 1707–1714 (2022).

46. Giannakis, S. Analogies and differences among bacterial and viral disinfection by the photo-Fenton process at neutral pH: a mini review. *Environ. Sci. Pollut. Res.* **25**, 27676–27692 (2018).

47. Jung, Y. J., Baek, K. W., Oh, B. S. & Kang, J. W. An investigation of the formation of chlorate and perchlorate during electrolysis using Pt/Ti electrodes: The effects of pH and reactive oxygen species and the results of kinetic studies. *Water Res.* **44**, 5345–5355 (2010).

48. Jha, D. & Bose, P. Use of pyrite for pH control during hydrogenotrophic denitrification using metallic iron as the ultimate electron donor. *Chemosphere* **61**, 1020–1031 (2005).

49. Lu, J. et al. Electrolysis-integrated constructed wetland with pyrite filler for simultaneous enhanced phosphorus and nitrogen removal. *Chem. Eng. J.* **451**, 138542 (2023).

50. World Health Organization. Disease Outbreak News; Cholera – Global situation. https://www.who.int/emergencies/disease-outbreak-news/item/2022-DON426 (2022).

51. Ward, M. H. et al. Drinking water nitrate and human health: an updated review. *Int. J. Environ. Res. Public Health* **15**, 1–31 (2018).

52. Wang, X., Prévoteau, A. & Rabaey, K. Impact of periodic polarization on groundwater denitrification in bioelectrochemical systems. *Environ. Sci. Technol.* **55**, 15371–15379 (2021).

53. Tammeaid, I. & Money, N. J. Elements of groundwater pollution and protection in a karst environment of Lusaka. In *International Mine Water Association Symposium 1993* 410–414 (International Mine Water Association (IMWA), 1993).

54. Bard, A. J. & Faulkner, L. R. *Electrochemical Methods: Fundamentals and Applications*. 2nd ed. (John Wiley & Sons, 2001).

55. Florentino, A. P., Costa, R. B., Hu, Y., O'Flaherty, V. & Lens, P. N. L. Long chain fatty acid degradation coupled to biological sulfidogenesis: a prospect for enhanced metal recovery. *Front. Bioeng. Biotechnol.* **8**, 1–14 (2020).

56. 3500-Fe B. Phenanthroline method. Standard Methods Online - Standard Methods for the Examination of Water and Wastewater. (Represents the most current version of the method, which was printed in the 24th edition of Standard Methods for the Examination of Water and Wastewater) http://standardmethods.org/ https://www.nemi.gov/methods/method_summary/7421/ (2023).

57. Nitrogen, Ammonia (Colorimetric, Automated Phenate). Methods for the Determination of Inorganic Substances in Environmental Samples (Revision 2.0. August 1993) (EPA/600/R-93/100) https://www.nemi.gov/methods/method_summary/5405/ (1993).

58. Alkalinity (Colorimetric, Automated, Methyl Orange). Methods for the Chemical Analysis of Water and Wastes (MCAWW) (EPA/600/4-79/020) https://www.nemi.gov/methods/method_summary/5231/ (1974).

59. APHA. APHA method 4500-Cl. In *Standard Methods for the examination of water and wastewater*, vol. 552 (APHA, 1992).

60. USEPA. *Analytical methods approved for compliance monitoring under the revised total coliform rule. Office of Water (MS – 4606 M), EPA 821-F-17-004* **852** (USEPA, 2017).

AUTHOR CONTRIBUTIONS

COMPETING INTERESTS

The authors declare no competing interests.

ADDITIONAL INFORMATION